In Situ TEM Investigation of $\langle c+a \rangle$ Dislocations in Magnesium

Bo-Yu Liu, Fei Liu, Bin Li, Jian-Feng Nie, and Zhi-Wei Shan

Abstract

The ductility of magnesium is intimately related to $\langle c+a \rangle$ dislocation. Understanding the behavior of $\langle c+a \rangle$ dislocations is of critical importance for resolving the mechanical properties and for alloy design. By using in situ TEM mechanical testing of pillars of pure Mg single crystal, we found that $\langle c+a \rangle$ dislocation can accommodate considerable plasticity. Our findings provide information on the mobility of $\langle c+a \rangle$ dislocation and its relationship with plasticity of submicron-sized pure Mg. The experimental strategy can be extended to understanding the dislocation behaviors in other hexagonal metals.

Keywords

Magnesium • In situ TEM • $\langle c+a \rangle$ dislocation • Plasticity

B.-Y. Liu · F. Liu · Z.-W. Shan (✉)
State Key Laboratory for Mechanical Behavior of Materials, Center for Advancing Materials Performance from the Nanoscale (CAMP-Nano) and Hysitron Applied Research Center in China (HARCC), Xi'an Jiaotong University, 710049 Xi'an, People's Republic of China
e-mail: zwshan@xjtu.edu.cn

B. Li
Department of Chemical and Materials Engineering, University of Nevada, Reno, USA

J.-F. Nie
Department of Materials Science and Engineering, Monash University, Melbourne, VIC 3800, Australia

International Joint Laboratory for Light Alloys (Ministry of Education), College of Materials Science and Engineering, Chongqing University, 400044 Chongqing, China

Introduction

Magnesium is the lightest structural metal, which is attracting worldwide interests because of its potential applications to higher energy efficiency and lower emissions by light weighting [1–4]. One bottleneck that hampers the widespread using of magnesium-based materials is their low ductility, which imposes severe constraints on cost-sensitive processing [5, 6]. The ductility of magnesium is closely related to pyramidal $\langle c+a \rangle$ dislocations [7]. $\langle c+a \rangle$ dislocation slip can provide plastic strain along the *c*-axis, which is necessary for accommodating anisotropic plasticity of magnesium undergoing plastic forming, e.g. rolling and drawing. Over the past decades, understanding the fundamental behaviors of $\langle c+a \rangle$ dislocations has been central to the research of ductility and formability of magnesium and its alloys [8–34]. Recent studies focus on whether $\langle c+a \rangle$ dislocations can glide and therefore to accommodate plastic strain [35–50]. This issue is of critical importance in determining the strategy for the development of new wrought magnesium alloys. Our recent work demonstrated that at least for submicron-size pure magnesium, pyramidal $\langle c+a \rangle$ dislocations of various characters (edge, screw, and mixed) can glide on both pyramidal I and II planes to generate large plasticity [50]. The current paper presents more experimental details and provides more experimental observations of mobile pyramidal $\langle c+a \rangle$ dislocations in single crystal magnesium.

Methods

In situ quantitative mechanical testing inside transmission electron microscope (TEM) can capture microstructure evolution in real time and obtain the corresponding mechanical data [50–55]. Figure 1 shows the sample preparation and experimental setup. The submicron-size pillars were fabricated by using focused ion beam (FIB). In situ TEM compression experiments were performed with a

J. B. Jordon et al. (eds.), *Magnesium Technology 2020*, The Minerals, Metals & Materials Series, https://doi.org/10.1007/978-3-030-36647-6_22

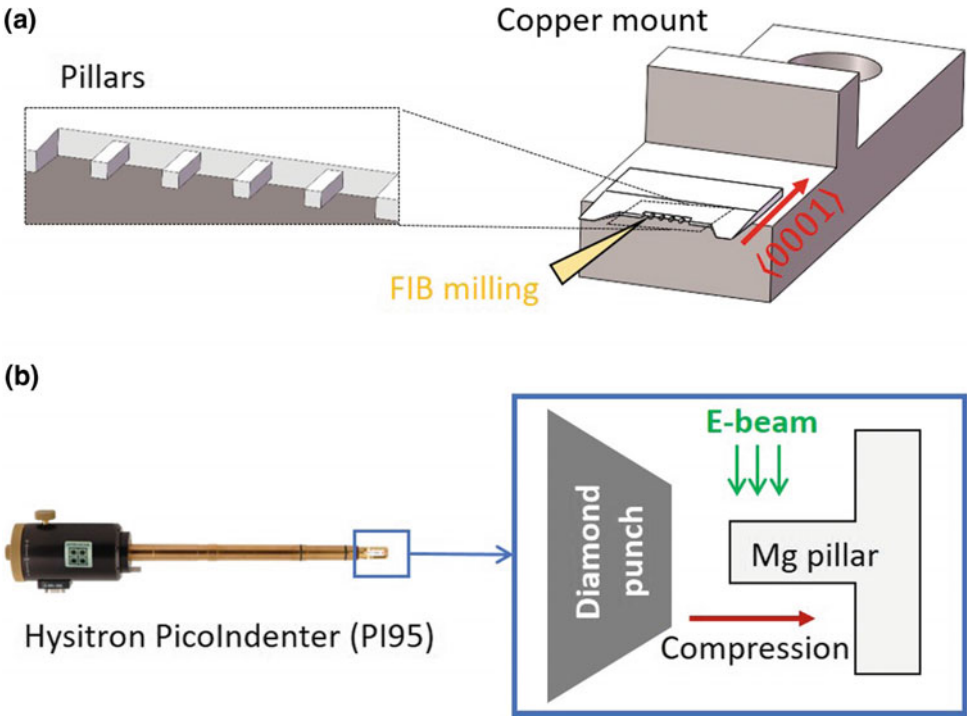

Fig. 1 Sample preparation and experimental setup. **a** The sample is pasted on a copper mount. The pillars are fabricated by FIB. **b** In situ TEM mechanical testing setup

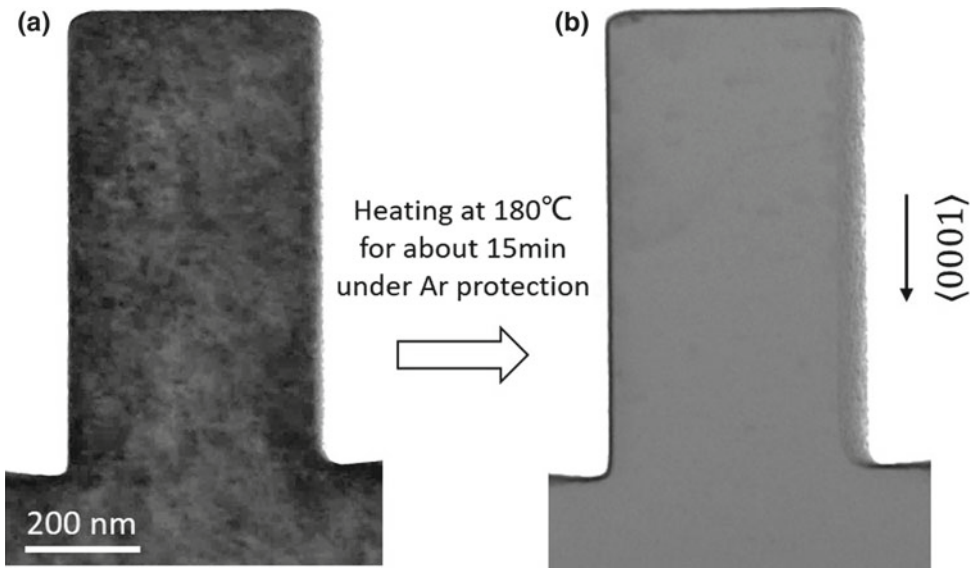

Fig. 2 FIB-induced defects can be largely reduced by annealing. **a** As-FIBed pillar. (b) Annealed pillar. Zone axis $\sim[2\bar{1}\bar{1}0]$

Hysitron PicoIndenter (PI95) inside a TEM (JEOL 2100F, 200 keV). In situ videos were recorded by Gatan 833 camera. The pillars were compressed by a diamond indenter with a flat punch. The compression tests were conducted under displacement control mode with the strain rate of 10^{-3} s^{-1}. The compressive loading direction is parallel to the axial direction of pillar that is close to $<0001>$. The viewing direction (zone axis) is $\sim<2\bar{1}\bar{1}0>$.

The FIB-induced defects on pillar surface will interfere with the contrast of dislocations. In order to reduce such interference, the samples were annealed at 180 °C for about 15 min inside a tube furnace. Argon atmosphere was used to protect the magnesium sample from oxidation. Figure 2 shows a pillar before and after annealing. In the as-FIBed pillar, there were FIB-induced defects which were largely removed after annealing.

Results

One typical example of pillar compression tests is shown in Fig. 3. The test was monitored under dark-field imaging condition with $g = \{0002\}$. In this imaging condition, only dislocations with Burgers vector containing $\langle c \rangle$ component were visible. These dislocations activated under c-axis compression were proven to be $\langle c+a \rangle$ dislocations by using $g \cdot \boldsymbol{b}$ contrast analysis [50]. The dislocations first appeared when the applied stress reached ~220 MPa. They formed near the contact interface between the pillar top and the diamond punch. More dislocations formed and gradually propagated through the entire pillar during the loading. The test was terminated at 7.1% strain. No failure was observed in this pillar. Note that higher plastic strains would be achievable if the tests continued. In the lower parts of this pillar, several $\langle c+a \rangle$ dislocations can be clearly observed (marked by dashed frame, Fig. 3c).

The glide of three dislocations is displayed in Fig. 4. The initial position of these dislocations is marked by a series of colored dots: dislocation-1, red; dislocation-2, green; dislocation-3, orange (Fig. 4a). According to our previous TEM characterizations and geometrical analyses, the long and straight segments lying parallel to the intersection of pyramidal plane and basal plane are of edge types, while the rest of segments are of mixed or screw types [50]. Figure 4b shows the schematic drawing of the moving dislocations in the corresponding TEM snapshots. The current and previous

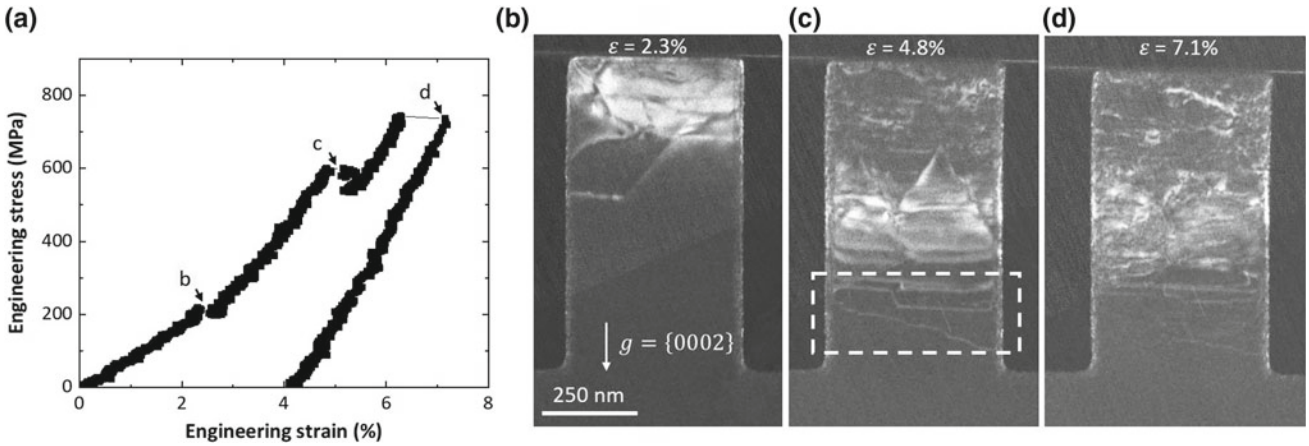

Fig. 3 In situ TEM mechanical testing shows that $\langle c+a \rangle$ dislocations are generated and glide during loading of a pillar. Loading direction, ~[0001]. Zone axis, $\sim [2\bar{1}\bar{1}0]$. **a** Corresponding engineering stress–strain curve. **b–d** Dark-field TEM images captured from in situ video show the formation and propagation of $\langle c+a \rangle$ dislocations. ε, engineering strain

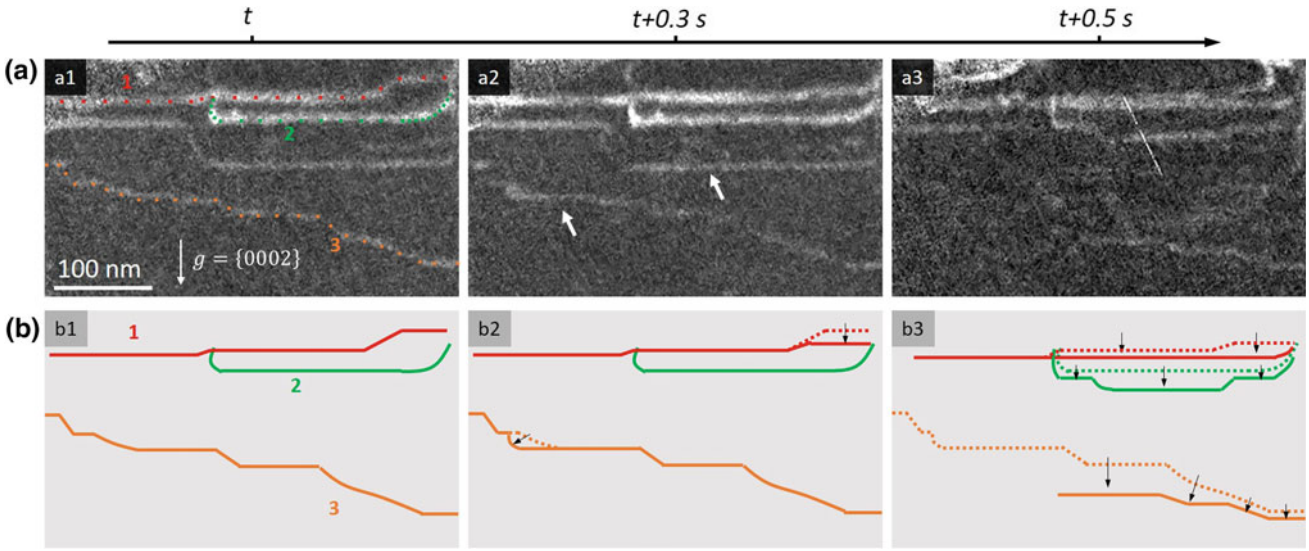

Fig. 4 In situ TEM observation shows the movement of $\langle c+a \rangle$ dislocations during loading. **a** A set of dark-field images captured from in situ movies with time sequence. Zone axis, $\sim [2\bar{1}\bar{1}0]$. **b** Schematic drawing of the moving dislocations in the corresponding TEM images

location of dislocations is represented by solid and dashed lines, respectively. The black arrows indicate the direction of dislocation movement. These dislocations exhibit zig-zag and half-loop configuration and therefore contain edge, screw, and mixed segments. The movement of these dislocations indicated that the $\langle c+a \rangle$ edge, screw, and mixed dislocation are all glissile, contributing to plastic deformation. The pure edge segments are also observed to glide under applied stress, indicating that they are glissile. We also note that some parts of the dislocations disappeared during loading (marked by white arrows in Fig. 4a). These parts may have moved out to the pillar surface.

Discussion

In submicron-sized crystals, the amount of preexisting dislocations should be less than that in bulk scale crystals. In the present work, the magnesium pillar was annealed, which further reduced the density of preexisting dislocations. Therefore, higher stress is needed to nucleate dislocations or activate dislocation sources in the submicron-sized magnesium pillars than that in larger pillars. For example, the yield stress for bulk and micron scale magnesium single crystal pillars under *c*-axis compression is in the range of 200–300 MPa [10, 21, 24]; when the sample size reduces to the submicron scale, the yield stress increases to 600–800 MPa [50]. Such high stresses can promote the formation and motion of $\langle c+a \rangle$ dislocations to accommodate plasticity. Note that the failure strain for bulk magnesium single crystal under *c*-axis compression is usually less than 10% [10, 21], but for submicron-size magnesium the plastic strain can be as high as 30% [50]. Moreover, in our submicron-size magnesium pillars, $\{10\bar{1}1\}$ contraction twin does not form. This deformation twinning mode often occurs in bulk scale magnesium under *c*-axis compression [56]. Contraction twins may introduce shear localization and stress concentration and serve as crack initiation sites. Therefore, the suppression of deformation twinning in small scale may also help prevent low-strain failure.

In magnesium and other hexagonal metals, $\langle c+a \rangle$ slip can provide extra independent slip systems to meet the von Mises criterion and can provide *c*-axis strain. In contrast, type $\langle a \rangle$ dislocations offer only four independent slip systems and cannot contribute to *c*-axis strain. Therefore, $\langle c+a \rangle$ dislocation slip is important in promoting uniformity in plastic strain accommodation and overall ductility in magnesium. Our results find that $\langle c+a \rangle$ dislocations are glissile and can contribute to considerable plasticity in submicron-size magnesium. This suggests that reducing grain size may be an effective way to improve the ductility of magnesium by promoting $\langle c+a \rangle$ dislocation slip.

Summary

By conducting in situ TEM mechanical testing, we have demonstrated that pyramidal $\langle c+a \rangle$ edge, screw, and mixed dislocations are glissile. They can serve as predominant plasticity carrier when a submicron-sized magnesium crystal undergoes *c*-axis compression. Our results are expected to provide new insights into the mechanical behavior of magnesium at different length scales.

Acknowledgements This work was supported by the National Key Research and Development Program of China (No. 2017YFB0702001), National Natural Science Foundation of China (Nos. 51601141), China Postdoctoral Science Foundation (2016M600788), and funding from the Science and Technology Departments of Shaanxi, China (Nos. 2016KTZDGY-04-03, 2016KTZDGY-04-04). B. L. thanks the support from US National Science Foundation (CMMI-1635088). J. F. N. acknowledges the support from the Australian Research Council.

References

1. L.-Y. Chen, et al., Nature (2015).
2. W. Xu, et al., Nat. Mater. (2015).
3. G. Wu, et al., Nature (2017).
4. T.M. Pollock, Science (2010).
5. B.-C. Suh, et al., Scr. Mater. (2014).
6. W.J. Joost, et al., Scr. Mater. (2017).
7. M.H. Yoo, Metall. Trans. A (1981).
8. H. Yoshinaga, et al., T. Jpn. I. Met. (1964).
9. J.F. Stohr, et al., Philos. Mag. (1972).
10. T. Obara, et al., Acta Metall. (1973).
11. S. Ando, et al., Non-Basal Slips in Magnesium and Magnesium-Lithium Alloy Single Crystals, Mater. Sci. Forum, 2000, pp. 1188-1191.
12. M.H. Yoo, et al., Mater. Sci. Eng., A (2001).
13. S.R. Agnew, et al., Metall. Mater. Trans. A (2002).
14. H. Tonda, et al., Metall. Mater. Trans. A (2002).
15. M.H. Yoo, et al., Metall. Mater. Trans. A (2002).
16. S.R. Agnew, et al., Scr. Mater. (2003).
17. J. Koike, et al., Acta Mater. (2003).
18. K. Mathis, et al., Acta Mater. (2004).
19. S.R. Agnew, et al., Int. J. Plast. (2005).
20. S. Agnew, et al., Acta Mater. (2006).
21. T. Kitahara, et al., Key Engineering Materials (2007).
22. O. Muránsky, et al., Mater. Sci. Eng. A (2008).
23. B. Li, et al., Philos. Mag. (2009).
24. C.M. Byer, et al., Scr. Mater. (2010).
25. B. Li, et al., Acta Mater. (2010).
26. E. Lilleodden, Scr. Mater. (2010).
27. B. Syed, et al., Scr. Mater. (2012).
28. Z. Yang, et al., Acta Mater. (2013).
29. J. Geng, et al., Philos. Mag. Lett. (2014).
30. H. Fan, et al., Mater. Sci. Eng. A (2015).
31. M. Itakura, et al., Phys. Rev. Lett. (2016).
32. K.Y. Xie, et al., Scr. Mater. (2016).
33. J. Jain, et al., Scr. Mater. (2017).
34. M.A. Shehadeh, et al., Comput. Mater. Sci. (2017).
35. S. Sandlöbes, et al., Acta Mater. (2011).
36. S.R. Agnew, Advances in Wrought Magnesium Alloys, Woodhead Publishing 2012, pp. 63-104.

37. S. Sandlöbes, et al., Acta Mater. (2012).
38. S. Sandlöbes, et al., Mater. Sci. Eng. A (2013).
39. Q. Yu, et al., Proc. Natl. Acad. Sci. (2013).
40. S. Sandlöbes, et al., Acta Mater. (2014).
41. Y. Tang, et al., Acta Mater. (2014).
42. S.R. Agnew, et al., Acta Mater. (2015).
43. Z. Wu, et al., Nature (2015).
44. Z. Wu, et al., Scr. Mater. (2016).
45. A. Kumar, et al., Mater. Sci. Eng. A (2017).
46. B. Li, et al., Scr. Mater. (2017).
47. S. Sandlobes, et al., Sci. Rep. (2017).
48. R. Ahmad, et al., Scr. Mater. (2018).
49. Z. Ding, et al., Acta Mater. (2018).
50. B.-Y. Liu, et al., Science (2019).
51. Z.W. Shan, JOM (2012).
52. B.Y. Liu, et al., Nat. Commun. (2014).
53. B.-Y. Liu, et al., Scr. Mater. (2015).
54. B.-Y. Liu, et al., J. Mater. Sci. Technol. (2018).
55. Y. Wang, et al., Nat. Commun. (2018).
56. M.R. Barnett, Mater. Sci. Eng. A (2007).